Vol 18 No 6, June 2009
1674-1056/2009/18(06)/2582-07

Chinese Physics B

Simulation of magnetization behaviours of Sm(Co,Fe,Cu,Zr)z magnet with low Cu content*

Chen Ren-Jie(陈仁杰)[a)c)†], Zhang Hong-Wei(张宏伟)[b)],
Shen Bao-Gen(沈保根)[b)], Yan A-Ru(闫阿儒)[a)], and Chen Li-Dong(陈立东)[c)]

[a)] *Ningbo Institute of Materials Technology & Engineering, Chinese Academy of Sciences, Ningbo* 315201, *China*
[b)] *State Key Laboratory of Magnetism, Institute of Physics and Center for Condensed Matter Physics, Chinese Academy of Sciences, Beijing* 100190, *China*
[c)] *Shanghai Institute of Ceramics, Chinese Academy of Sciences, Shanghai* 200050, *China*

(Received 17 September 2008; revised manuscript received 28 November 2008)

The effects of microstructure, cell orientation and temperature on magnetic properties and the coercivity mechanism in Sm(Co,Fe,Cu,Zr)z with low Cu content are studied by using the micromagnetic finite element method in this paper. The simulations of the demagnetization behaviours indicate that the pinning effect weakens gradually with the thickness of cell boundary decreasing and strengthens gradually with the cell size decreasing. Because of the intergrain exchange coupling, the coercivity mechanism is determined by the difference in magnetocrystalline anisotropy between the cell phase and the cell boundary phase. And the coercivity mechanism is related to not only the cells alignment but also temperature. With temperature increasing, a transformation of the demagnetization mechanism occurs from the domain pinning to the uniform magnetization reversal mode and the transformation temperature is about 650 K.

Keywords: micromagnetic finite element method, microstructure, cell orientation, temperature
PACC: 7550V, 7560V, 7560G

1. Introduction

The precipitation-hardened Sm(Co,Fe,Cu,Zr)z permanent magnets (PMs) have re-attracted much attention due to their very excellent high temperature magnetic properties since the 1990s.[1−6] These excellent magnetic properties are considered to be related to the complex cellular microstructure, which consists of 2:17 rhombohedral cells each with a size around 100 nm, surrounded by 10 nm 1:5 cell boundaries.[1,7−9] Recently, many research results indicated that the different temperature dependences of coercivity had been discovered in this kind of PM.[1,3−5,10] It is universally received that the coercivity mechanism is controlled by domain wall pinning in this kind of PM, which is determined by the difference in domain wall energy density between the two phases. According to the temperature dependence of coercivity, the Sm(Co,Fe,Cu,Zr)z PMs are distinguished from the traditional Sm(Co,Fe,Cu,Zr)z PMs and the modern Sm(Co,Fe,Cu,Zr)z PMs.[3,10] The coercivity of the former deteriorates rapidly and monotonically with temperature increasing, but the latter exhibits an abnormal temperature dependence of coercivity in a certain temperature range. There are several models to explain the temperature dependence of mechanism of coercivity in Sm(Co,Fe,Cu,Zr)z. And the Cu content in cell boundary phase plays an important role in mechanism and its temperature dependence.[1,3−6,11] If the Cu content in cell boundaries is large enough to make the cell boundary nonmagnetic, the mechanism of coercivity should be controlled by nucleation. But if the Cu content is too low, the cell boundary should be magnetic and the magnetization behaviour becomes very complicated because of the complex microstructure. And thus, the mechanism of coercivity is unclear in Sm(Co,Fe,Cu,Zr)z PMs with low Cu content.

Micromagnetics based on the continuum theory is suitable for the investigation of the magnetization behaviour in a magnet. Recently, the micromagnetic finite-element method (FEM), in which the theory of micromagnetics and the finite-element method combine together, is confirmed to be effective for

*Project supported by the Natural Science Foundation of Zhejiang Province, China (Grant No Y407174).
†Corresponding author. E-mail: chenrj@nimte.ac.cn

the simulation of a magnetization distribution under a magnetic field.[12−15] So, three-dimensional (3D) micromagnetic FEM simulation is usually used to analyse the magnetic behaviour in PMs.[16−21] We have studied the mechanism of magnetization reversal in Sm(Co,Fe,Cu,Zr)z PMs with high Cu content through the micromagnetics FEM simulation.[19−21] In the present paper, the magnetization behaviours of Sm(Co,Fe,Cu,Zr)z PMs with low Cu content are investigated systematically through the micromagnetics FEM simulation using the software package Magpar,[22] and the simulation is described in reference [12]. The effects of microstructure, cells orientation and temperature on magnetic properties and coercivity mechanism are studied in the present paper.

2. The simulation model

According to the continuum micromagnetic theory, the total magnetic Gibbs free energy of a system is composed of the Zeeman energy $\Phi_{\rm H}$, the dipolar energy $\Phi_{\rm D}$, the anisotropic energy $\Phi_{\rm K}$ and the exchange energy $\Phi_{\rm ex}$,[23,24] i.e.,

$$G = \Phi_{\rm H} + \Phi_{\rm D} + \Phi_{\rm K} + \Phi_{\rm ex}. \quad (1)$$

This expression is a function of the direction of the spontaneous polarization $J_{\rm s}$, and the magnetization distribution can be obtained by minimizing the Gibbs free energy. The long-range dipolar–dipolar interaction is solved by introducing a magnetic vector potential. A more detailed description about this method is given in reference [12].

The investigation of the microstructure Sm(Co,Fe,Cu,Zr)z PMs by the transmission electron microscopy reveals that the regular rhombohedral cellular 2:17 phase cell (about 100 nm in size) is surrounded by the 1:5 phase cell boundary (about 10 nm in thickness).[3−5,25,26] Therefore, a cubic model consisting of $5 \times 5 \times 5$ cells is built in the present paper. Figure 1 gives the simulation model. As shown in figure 1, the small cubes represent the Sm_2Co_{17}-type cells, each of which is surrounded by the $SmCo_5$-type cell boundaries. The effects of microstructure and temperature on demagnetization behaviour are studied by simulating the demagnetization process, changing the microstructure parameters (the sizes of cell phase and cell boundary) and magnetic parameters for different temperatures. And the influence of cell alignment degree on demagnetization behaviour is also studied. The mean direction of a sample is fixed on the Z-axis which is parallel to the field direction. And the standard deviation σ is adopted to describe the orientation degree of every cell. And the standard deviation σ is adopted to describe the orientation degree of each cell. A detailed description is given in reference [27].

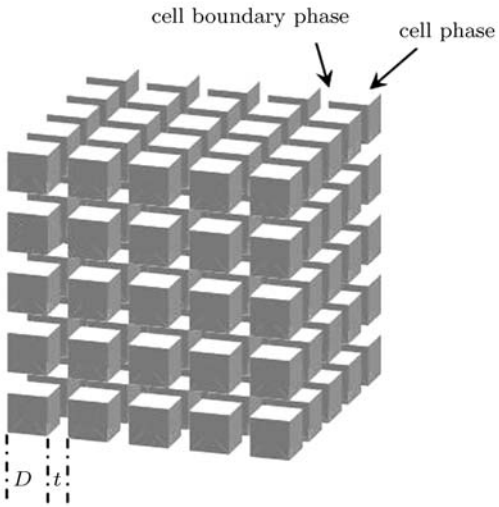

Fig.1. Simulation model composed of 125 cells.

At room temperature (RT), the cell size D varies from 30 nm to 50 nm, with fixing cell boundary thickness $t = 6$ nm, and the cell boundary thickness changes from 2 nm to 8 nm with fixing cell size $D = 50$ nm. The RT magnetic parameters of the cell phase ($J_s^{2:17} = 1.24$ T, $K_1^{2:17} = 2.9$ M·J/m^3, $A^{2:17} = 9.5 \times 10^{-12}$ J/m) and cell boundary phase ($J_s^{1:5} = 0.66$ T, $K_1^{1:5} = 8.1$ M·J/m^3, $A^{1:5} = 7.7 \times 10^{-12}$ J/m) as reported in reference [28] are used in the present simulation. Because of the low Cu content in the cell boundary phase, one can find that the magnetocrystalline anisotropy of the cell boundary is much larger than that of the cell phase. And the saturation magnetization $J_{\rm s}$ of the sample is dependent on the fractions of two phase volumes and related to microstructure as well. The magnetic parameters at high temperatures are deduced through the following equations:

$$\begin{aligned} J_{\rm S}(T) &= C_{\rm J}(1 - T/T_{\rm C})^{\beta}, \\ K_1(T) &= C_{\rm K}(J_{\rm S}(T))^3, \\ A(T) &= C_{\rm A}(J_{\rm S}(T))^2. \end{aligned} \quad (2)$$

Here, $\beta = 0.5$ for the molecular field theory and $\beta = 0.365$ for 3D Heisenberg model. And we adopt the former in this work.

3. Results and discussion

3.1. Influence of microstructure

Figure 2 shows the curves for simulated demagnetization versus coercivity for several cell sizes at RT. In figure 2(a), the cell size D is 50 nm and the cell boundary t changes from 2 nm to 8 nm. The coercivity $\mu_0 H_c$ increases from 2.88 T at $t = 2$ nm to 4.16 T at $t = 8$ nm, but it should not increase obviously when $t \geq 6$ nm. It is contrary to the relationship between coercivity and cell boundary thickness in traditional Sm(Co,Fe,Cu,Zr)z PMs with high Cu content. Because of the low Cu content in cell boundaries, the magnetic anisotropy is stronger in the cell boundaries than that in the cell phase. And the intergrain exchange coupling (IGEC) makes the nucleation field increase in the cell phase, i.e. the cell phase is magnetically hardened by the neighbouring cell boundary phase as done in hard/soft nanocomposite PMs. When the cell boundary thickness t is less than 6 nm, the demagnetization curve shows a single phase PM and no domain wall pinning effect. But a plateau in the demagnetization curve indicates a two-phase demagnetization behaviour and a domain wall pinning process at $t = 8$ nm. Because the anisotropy in the cell boundary is stronger than that in the cell phase, the magnetic reversal starts with the nucleation of a reversal domain in the cell phase and the domain wall is pinned in the cell phase. In the simulation results given by Scholz *et al*,[29,30] the similar phenomenon to the relationship between the effect of domain wall pinning and the thickness of the cell boundary is observed.

Figure 2(b) shows the curves for simulated demagnetization for several cell sizes at cell boundary $t = 6$ nm at RT. The domain wall pinning effect can be observed from all demagnetization curves from $D = 30$ nm to 50 nm. This indicates that the demagnetization processes are controlled by the domain wall pinning. Although the coercivity $\mu_0 H_c$ has almost no change with cell size D decreasing from 50 nm to 35 nm, it increases sharply to 4.97 T when the cell boundary size is 30 nm. It results from two factors: one is the nucleation field increasing due to the IGEC as mentioned above and the other is the relative volume of the IGEC effect v_{ex} increasing with the cell size decreasing. In this paper, the v_{ex} is defined as follows:

$$v_{ex} = \left[\left(D + \delta_B^{1:5}\right)^3 - \left(D - \delta_B^{2:17}\right)^3\right]/(D+t)^3, \quad (3)$$

where $\delta_B^{1:5}$ and $\delta_B^{2:17}$ are the theoretical thicknesses of domain walls in the cell boundary phase and in the cell phase, respectively. Accordingly our simulation results about the microstructure and the impulsive domain wall pinning are related not only to the cell boundary thickness, but also the cell size, i.e. the relative volume v_{ex} of the IGEC effect.

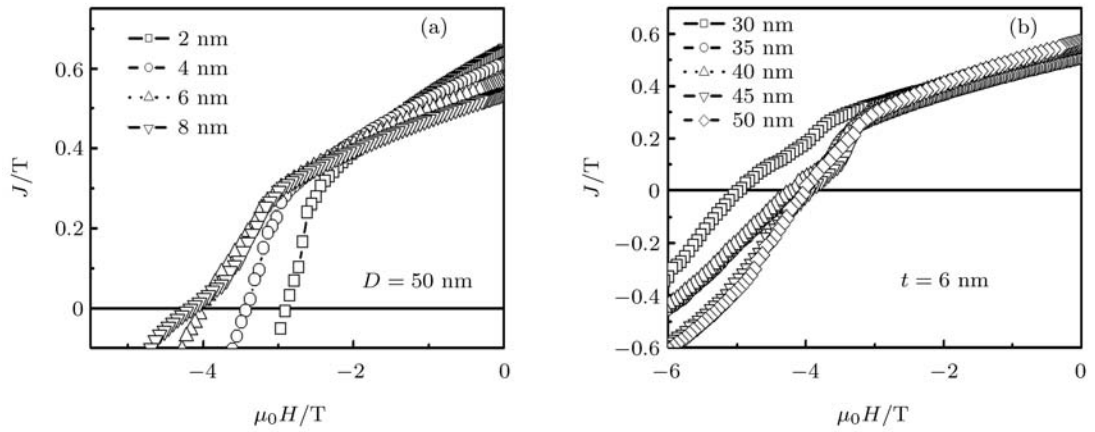

Fig.2. Curves for simulated demagnetization versus coercivity for several different cell boundary sizes (a) and cell sizes (b).

3.2. Influence of cell alignment

In order to study the influence of the cell alignment on demagnetization behaviour, the demagnetization processes are simulated versus orientation distribution of the crystalline anisotropy field in different cells, with different standard deviation degrees of easy axis, i.e. $\sigma = 0°$, $5°$, $10°$, $15°$, $20°$ and $30°$, and 2:17 cell size $D = 50$ nm, and 1:5 cell boundary $t = 6$ nm. The demagnetization curves are shown in figure 3 with the value of σ varying from $0°$ to $30°$ in steps of $5°$.

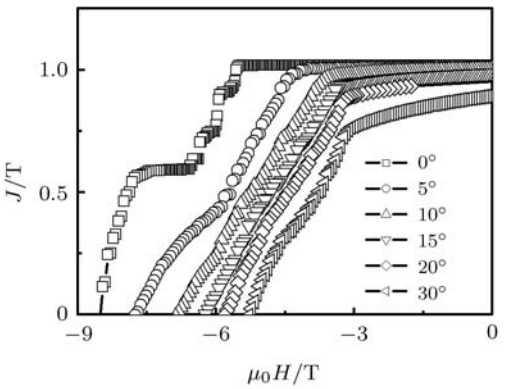

Fig.3. Demagnetization curves for different cell alignment degrees.

For the ideal anisotropic magnet, $\sigma = 0°$ and the demagnetization curve shows an observable plateau at external field $\mu_0 H \approx 6$ T, which is greater than the theoretical nucleation field 5.87 T of the cell phase 2:17 but less than that of the cell boundary phase 1:5. On the one hand, the cell phase is magnetically hardened by the boundary phase which results in the increase of nucleation field. On the other hand, the domain wall is pinned in the boundary phase due to the higher magnetic crystalline anisotropic field than that of the cell. With the deterioration of the cell alignment, the plateau disappears rapidly in the demagnetization curve which indicates that the coercivity mechanism changes from homogeneous pinning to inhomogeneous pinning. It is consistent with our previous simulation results[21] where the coercivity mechanism was related to the crystalline orientation.

Figure 4 shows the curves for remanence ratio m_r, coercivity $\mu_0 H_c$ and maximum energy product $(BH)_{max}$ versus standard deviation σ, and the theoretical m_r in the Stoner–Wohlfarth model is also shown in figure 4(a) for comparison. The value of m_r monotonically decreases with the value of σ increasing, which results from the deviation of magnetic moments from the direction of the external field because of the magnetic crystalline anisotropy in the remanence state. The nucleation field decreases with the deviation from easy axis, which makes the coercivity decrease. According to the simulation results, IGEC leads the value of m_r to be larger than that in the Stoner–Wohlfarth model (the remanence enhancement effect) and the coercivity to be larger than the cell phase nucleation field $\mu_0 H_c = 5.87$ T when $\sigma \leq 15°$ as shown in figure 4(a). Because the value of $\mu_0 H_c$ is much larger than $J_r/2$, the value of $(BH)_{max}$ is determined by the J_r and the dependence of energy product on σ is similar to that of m_r on σ (figure 4(b)). In addition, the squareness of the demagnetization curve deteriorates with the value of σ increasing as shown in figure 3, which makes the value of $(BH)_{max}$ decrease too. Obviously, the cell alignment optimization is an effective way to improve the magnetic properties of PMs.

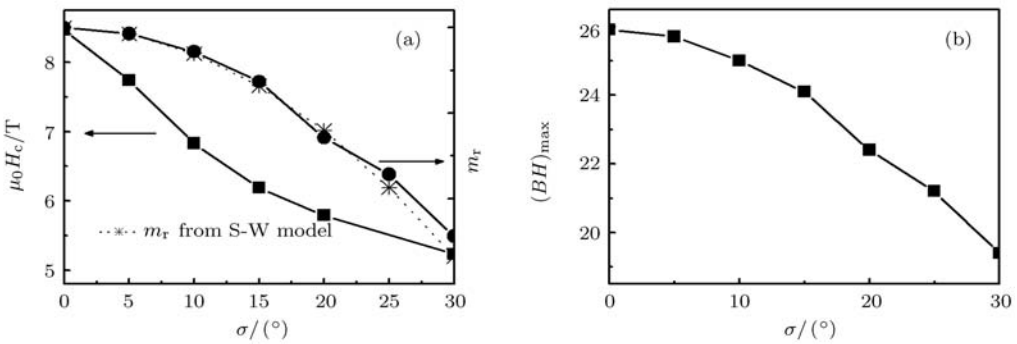

Fig.4. Remanence ratio m_r, coercivity $\mu_0 H_c$ (a) and maximum energy product $(BH)_{max}$ (b) versus standard deviation σ.

4. Simulations of demagnetization at different temperatures

Figures 5(a) and 5(b) show the demagnetization curves of anisotropic and isotropic magnets at different temperatures for $D = 50$ nm and $t = 6$ nm, respectively. For anisotropic magnet, the demagnetization curves each have a plateau at lower temperatures. This phenomenon is caused by the fact that the domain wall homogeneous pinning effect gradually weakens with temperature T increasing and even disappears at $T > 500$ K as shown in figure 5(a). However, no plateau can be observed in the whole temperature range under study for isotropic magnet as shown in figure 5(b). And comparing figure 5(a) with figure 5(b), one can find that the nucleation field of the anisotropic sample is much larger than the coercivity of isotropic sample at the same temperature. It maybe indicates that the coercivity mechanism is controlled by inhomogeneous domain wall pinning or magnetic moment reversal in the isotropic sample. As mentioned above, the coercivity mechanism is related to the crystalline orientation. In the isotropic sample, the depinning fields of the cells with different orientations are different, or even the progress of demagnetization is totally controlled by the magnetic moment reversal in some cells. This leads the plateau to disappear in the demagnetization curve as shown in figure 5(b).

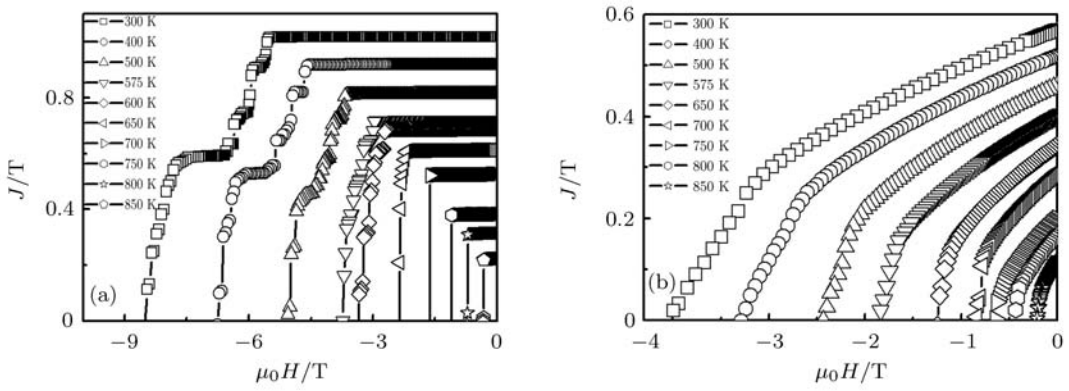

Fig.5. Demagnetization curves for anisotropic (a) and isotropic samples (b) at different temperatures.

According to the theory of domain wall pinning,[5,11,31,32] the coercivity mechanism should change from the repulsive model to the attractive model, if the domain wall energy density of 1:5 cell boundary phase $\gamma_{1:5}$ changes from larger to less than that of 2:17 cell phase $\gamma_{2:17}$ with temperature increasing. At the critical transition temperature (about 575 K in this work), $\gamma_{1:5}$ is equal to $\gamma_{2:17}$ and the domain walls undergo a motion subject to no resistance. But the domain wall pinning can be observed in the demagnetization curve at $T = 575$ K and the pinning effect disappears at $T = 650$ K as shown in figure 5(a). Obviously, the demagnetization mechanism becomes of uniform rotation model when temperature is higher than 650 K in which range the magnetocrystalline anisotropy constant of the cell phase $K_1^{2:17}$ is very close to that of the cell boundary phase $K_1^{1:5}$. That indicates that the pinning field is determined by the difference in magnetocrystalline anisotropy ΔK_1 between the cell phase and the cell boundary phase. At $T > 650$ K, $\Delta K_1 < 0.4 \times 10^6$ J/m^3, the demagnetization process is controlled by the uniform rotation in the cell phase and the pinning effect disappears as shown in figure 5(a). Similar phenomena were reported by Scholz *et al.*[29,30]

Figure 6 shows the magnetization distributions in the demagnetization process for the anisotropic sample at 500 K. The magnetization reversal occurs in the centres of the cells firstly due to the action of lower anisotropic field. And the outer moments of the cells keep in their magnetization states even when the external field increases to 4.85 T (1.235 times the anisotropic field of the cell phase) as shown in figure6 (a), which is due to the magnetic hardening effect coming from the cell boundary phase. With external field increasing, these demagnetization nucleations propagate and the magnetization areas are compressed and then the domain walls move into the cell boundary phase but are pinned at the cell boundary, which results in the plateaus of the demagnetization curves as shown in figure 5(a). With external field further increasing, the magnetic moments of the cell boundary phase further cause the reversal and only the moments in the corners of the cell boundaries keep in their magnetization states when the external field reaches to 8.27 T (see figure 6(d)). Obviously, in the

demagnetization process the magnetization reversal mechanism is controlled by the domain wall pinning at the cell boundary according to the magnetization distribution in the demagnetization process.

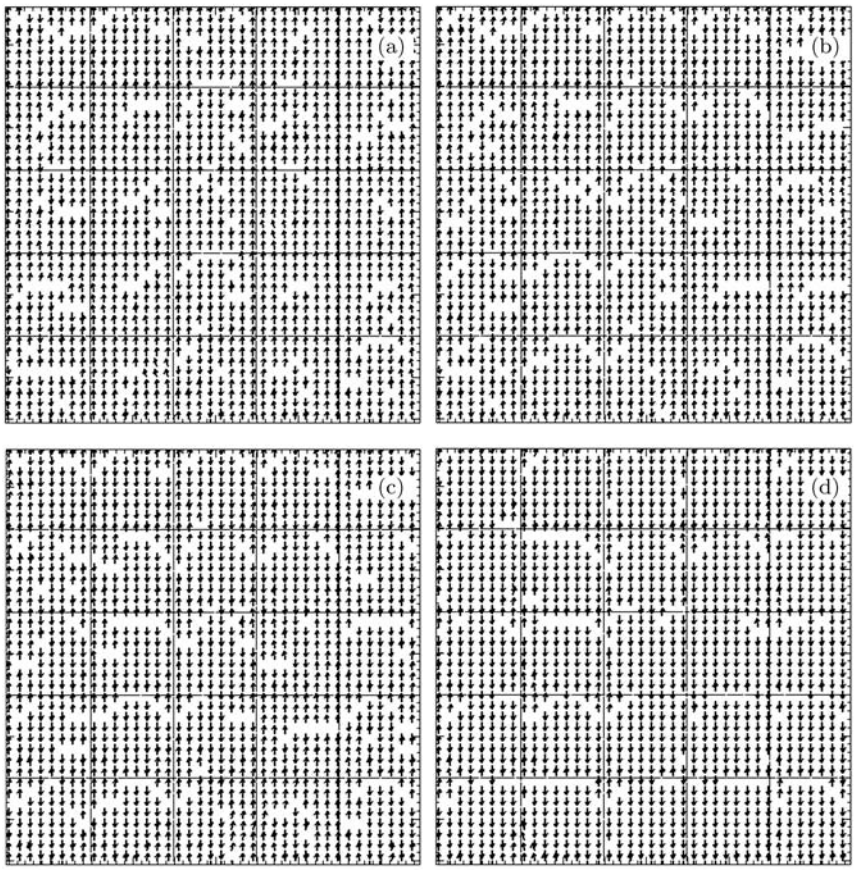

Fig.6. Magnetization distributions in demagnetization process for anisotropic sample at 500 K under external fields of 4.85 T (a), 5.05 T (b), 5.17 T (c) 8.27 T (d) separately.

5. Conclusion

The effects of microstructure, cells orientation and temperature on magnetic properties and coercivity mechanism in Sm(Co,Fe,Cu,Zr)z with low Cu content are studied by using the micromagnetic FEM. Because the magnetocrystalline anisotropy of the cell boundary phase is stronger than that of the cell phase at RT, the pinning effect weakens gradually with the thickness of cell boundary decreasing, and strengthens gradually with the cell size decreasing. The IGEC leads the magnetic moments of the cell phase to be hardened and the coercivity to be higher than the theoretical nucleation field of the cell phase. The study of the cells alignment influence indicates that the coercivity mechanism is related to the cell alignment and the magnetic properties deteriorate with σ increasing. Because of the IGEC, the coercivity mechanism is determined by the difference in magnetocrystalline anisotropy ΔK_1 rather than the difference in domain wall energy density $\Delta\gamma$ between the cell phase and the cell boundary phase. With the increase of temperature, a transformation of the demagnetization mechanism occurs from the domain pinning to the uniform magnetization reversal mode and the transformation temperature is about 650 K in this work.

References

[1] Popov A G, Korolev A V and Shchegoleva N N 1990 *Phys. Met. Metall.* **60** 100

[2] Liu J F, Ding Y and Hadjipanayis G C 1999 *J. Appl. Phys.* **85** 1670

[3] Hadjipanayis G C, Tang W, Zhang Y, Chui S T, Liu J F, Chen C and Kronmüller H 2000 *IEEE Trans. on Magn.*

36 3382
[4] Goll D, Kleinschroth I, Sigle W and Kronmüller H 2000 *Appl. Phys. Lett.* **76** 1054
[5] Zhou J, Shomski R, Chen C, Hadjipanayis G C and Sellmyer D J 2000 *Appl. Phys. Lett.* **77** 1514
[6] Gabay A M, Tang W, Zhang Y and Hadjipanayis G C 2001 *Appl. Phys. Lett.* **78** 1595
[7] Tang W, Zhang Y and Hadjpanayis G C 2000 *IEEE Trans. on Magn.* **36** 3294
[8] Zhang Y, Tang W, Hadjpanayis G C, Chen C, Nelson C and Krishnan K 2001 *IEEE Trans. on Magn.* **37** 2525
[9] Chen X, Liu J F, Ni C, Hadjipanayis G C and Kim A 1998 *J. Appl. Phys.* **83** 7139
[10] Liu J F, Chui T, Dimitrov D and Hadjipanayis G C 1998 *Appl. Phys. Lett.* **73** 3007
[11] Chui S T 2000 *J. Magn. Magn. Mater.* **217** 120
[12] Schrefl T, Fidler J and Kronmüller H 1994 *J. Magn. Magn. Mater.* **138** 15
[13] Fischer R and Kronmüller H 1996 *Phys. Rev.* B. **54** 7284
[14] Fischer R, Leineweber T and Kronmüller H 1998 *Phys. Rev.* B **57** 10723
[15] Zhang H W, Rong C B, Du X B, Zhang J, Zhang S Y and Shen B G 2003 *Appl. Phys. Lett.* **82** 4098
[16] Rong C B, Zhang H W, Zhang J, Du X B, Zhang S Y and Shen B G 2004 *J. Appl. Phys.* **95** 1351
[17] Rong C B, Zhang H W, Du X B, Zhang J, Zhang S Y and Shen B G 2004 *J. Magn. Magn. Mater.* **277** 221
[18] He S L, Zhang H W, Rong C B, Chen R J and Shen B G 2005 *Chin. Phys.* **14** 1055
[19] Chen R J, Rong C B, Zhang H W, He S L, Zhang S Y and Shen B G 2004 *Acta Phys. Sin.* **53** 4341 (in Chinese)
[20] Chen R J, Zhang H W, Rong C B, Sun J R and Shen B G 2006 *J. Magn. Magn. Mater.* **305** 191
[21] Chen R J, Zhang H W, Rong C B, Sun J R and Shen B G 2006 *J. Appl. Phys.* **100** 043901
[22] Scholz W, Fidler J, Schrefl T, Suess D, Dittrich R, Forster H and Tsiantos V 2003 *Comp. Mat. Sci.* **28** 366
[23] Brown W F Jr 1963 *Micromagnetics* (New York: Wiley-Interscience)
[24] Schrefl T, Fidler J and Kronmüller H 1994 *Phys. Rev.* B **49** 6100
[25] Liu S, Yang J, Doyle G, Kuhl E, Chen C H, Walmer M S and Simon G 1999 *IEEE Trans. on Magn.* **35** 3325
[26] Liu S, Yang G, Goyle G, Potts G and Kuhl G E 2000 *J. Appl. Phys.* **87** 6728
[27] He S L, Zhang H W, Rong C B, Chen R J, Sun J R and Shen B G 2005 *Acta Phys. Sin.* **54** 3408 (in Chinese)
[28] Goll D, Müller K H, and Stadelmaier H H 2004 *J. Appl. Phys.* **96** 6534
[29] Scholz W, Fidler J, Schrefl T, Suess D and Matthias T 2002 *J. Magn. Magn. Mater.* **242-245** 1356
[30] Scholz W, Fidler J, Schrefl T, Suess D and Matthias T 2002 *J. Appl. Phys.* **91** 8492
[31] Livingston J D and Martin D L 1977 *J. Appl. Phys.* **48** 1350
[32] Nagel H 1979 *J. Appl. Phys.* **50** 1026

低失重烧结钕铁硼磁体的研究进展

丁 勇*, 陈仁杰, 闫阿儒, 李 东
(中国科学院宁波材料技术与工程研究所, 浙江省磁性材料及其应用技术重点实验室, 浙江 宁波 315201)

摘要: 烧结钕铁硼永磁材料被发明以来, 以其优越的磁性能得到了广泛的应用, 目前成为永磁产业的支柱。但是其耐腐蚀性能差, 大大限制了其使用范围。因此, 近 20多年来如何改善其抗腐蚀性能成为烧结钕铁硼材料生产和使用的重要问题。总结了烧结钕铁硼腐蚀失重的机制, 制备低失重烧结钕铁硼的方法和工艺, 对如何提高烧结钕铁硼磁体的耐腐蚀性, 降低腐蚀失重进行了综述。从磁体成分设计和微观结构方面总结了几条提高烧结钕铁硼磁体耐蚀性的原则, 其关键是对晶界相的成分和微观结构进行合理的控制。

关键词: 烧结钕铁硼; 耐蚀性; 低失重
doi: 10.3969/j.issn.0258-7076.2010.01.029
中图分类号: TG132.2 **文献标识码**: A **文章编号**: 0258-7076(2010)01-0145-06

Progress of Sintered NdFeB Magnets with Low Weight Loss

Ding Yong*, Chen Renjie, Yan Aru, Lee Don
(Zhejiang Province Key Laboratory of Magnetic Materials and Application Technology, Ningbo Institute of Materials Technology and Engineering, Chinese Academy of Sciences, Ningbo 315201, China)

Abstract: Sintered NdFeB magnets were applied widely because of their excellent magnetic performance. At present, NdFeB magnets were the key materials in permanent magnet industry. Their poor corrosion resistance, however, was a major impediment for application. So, how to improve corrosion resistance was a key point for sintered NdFeB manufacture and application. The corrosion weight loss mechanism of sintered NdFeB magnets and the process for producing low weight loss of sintered NdFeB magnets were summarized. An overview how to improve corrosion resistance and reducing weight loss was outlined. It was found that composition and microstructure control of grain boundaries phase was a key point for low weight loss sintered NdFeB magnets.

Key words: sintered NdFeB; corrosion resistance; low weight loss

NdFeB永磁材料自 1983年诞生以来由于其突出的磁性能而被深入研究和广泛的应用, 它的发展带动了整个下游产业, 如通讯、电子、医疗和汽车行业的进步和产品更新, NdFeB产业已成为国民经济发展的重要组成部分。烧结钕铁硼具有优异的磁性能, 但是其抗腐蚀性能较差, 大大地限制了它的应用范围, 因此, 如何改善其抗腐蚀性能成为烧结钕铁硼材料生产和使用的重要问题。

钕铁硼系永磁体的腐蚀主要来源于两个方面: 一是氧化腐蚀; 二是电化学腐蚀。测定氧化腐蚀的速度有两种: 一种是增重法, 即测量腐蚀过程中磁体质量的增加; 另一种方法是失重法, 即在腐蚀过程, 将腐蚀产物清除, 然后测量磁体质量的减少 (即质量损失)。通常采用加速实验法来测量其腐蚀速度。

最近 20年以来人们对提高烧结钕铁硼的耐腐蚀性, 降低失重做了大量的工作, 取得了很大的进展。但是目前还没有专门的烧结钕铁硼低失重综述性的文献, 本文在总结了提高烧结钕铁硼耐蚀性的基础上, 对低失重烧结钕铁硼进行了综述, 提出了合理设计低失重烧结钕铁硼实验的原则。

收稿日期: 2009-08-10; **修订日期**: 2009-09-10
基金项目: 浙江省科技厅面上科研工业项目 (2007C21097)资助; 浙江省科技攻关项目 (2007C11046)资助和宁波市攻关项目 (2008B10024)资助
作者简介: 丁 勇 (1981-), 男, 安徽宣城人, 博士研究生, 研究方向: 稀土永磁材料
*通讯联系人 (E-mail: dingyong@nimte.ac.cn)

1 烧结钕铁硼腐蚀失重机制

烧结 NdFeB 磁体耐腐蚀性能差主要有以下 3 个原因:

(1) 材料自身的结构。烧结 NdFeB 永磁合金具有多相组织,且各相的氧化能力不同,分布在晶界处的富 Nd相和富 B相易于优先发生氧化,形成晶间腐蚀。另外磁体的致密度不高,加上氧化物较疏松,孔隙率大,磁体的表面很难形成氧化物保护膜,一旦氧化就造成连锁反应,加速氧化。而且由于磁体主相 $Nd_2Fe_{14}B$相的体积分数一般都在 90%以上,当形成电化学局部腐蚀电池时,具有小阳极大阴极的特点,晶界处富 Nd相和富 B相的腐蚀电流密度较大,加速了晶间腐蚀和破坏。

(2) 合金中存在的杂质。烧结 NdFeB 永磁合金中可能存在的污染杂质主要有 O, H, N, C, Si, Cl及氯化物等,其中对腐蚀性能危害最严重的是氧、氯和氯化物。磁体的腐蚀主要表现为氧化过程,而氯及氯化物特别是氯化钠的污染将加速磁体的氧化过程。

(3) 工作的环境。温度环境、介质条件以及湿度和压力等对磁体的腐蚀行为有较大的影响。钕铁硼磁体是由主相 $Nd_2Fe_{14}B$、富硼相 $Nd_{1+\xi}Fe_4B_4$和富钕相组成的多相合金,富钕相作为晶界相包围着主相,而富硼相绝大多数也存在于晶界中以及晶界交汇处。这些区域是易发生腐蚀的区域。烧结 NdFeB磁体容易发生腐蚀失重,一方面是由于元素 Nd是化学活性最高的金属元素之一[1],其标准电势 $E_0(Nd^{3+}/Nd) = -2.431$ V; 另一方面与磁体的多相结构以及各相间电化学电位的差异有关[2]。研究结果表明,NdFeB磁体的腐蚀主要发生在以下两种环境中:

高温环境。在干燥的环境下,当温度低于 150 ℃时,NdFeB磁体的氧化速度很慢,但在较高的温度下,富 Nd区会发生如下反应[3,4]:

$$4Nd + 3O_2 = 2Nd_2O_3 \quad (1)$$

随后,$Nd_2Fe_{14}B$相会分解生成 Fe和 Nd_2O_3。进一步氧化,还将出现 Fe_2O_3等产物,使其磁性能下降。

湿热环境。在湿热的条件下[5~7],NdFeB永磁体表层的富 Nd晶界相首先与水蒸气按下式发生腐蚀反应:

$$3H_2O + Nd = Nd(OH)_3 + 3H \quad (2)$$

反应生成的原子 H渗入到晶界中,与富 Nd相发生进一步的反应,造成晶界的腐蚀,其反应式如下:

$$Nd + 3H = NdH_3 \quad (3)$$

NdH_3相的生成会使晶界相的体积发生膨胀,造成晶界应力,导致晶界破坏和 $Nd_2Fe_{14}B$主相的迁移,严重时会使晶界发生断裂而造成磁体的粉化失效。而在潮湿的环境中生成的氢氧化物或其他含氢化合物则不具备这种保护作用,特别是当环境湿度过大时,磁体表面有液态的水存在时,将会发生电化学腐蚀[8]。Chang等[9,10]研究了 NdFeB合金在水溶液中的吸氢行为对腐蚀的影响。研究表明,吸氢量随着合金中稀土元素总含量的升高而增多,且腐蚀速率随着吸氢量的增多而增加。文献[11]中也提到了同样的结果。NdFeB永磁体发生电化学腐蚀时,各相的电化学电位不同,富钕相和富硼相相对于 $Nd_2Fe_{14}B$主相来说作为阳极,将会优先发生腐蚀[12,13],形成局部腐蚀的微电池,由于阳极相与阴极相的体积差别较大,这种微电池具有小阳极大阴极的特点,少量的富钕相和富硼相作为阳极承担了很大的腐蚀电流密度,而它们是分布于晶界处的,这样就加速了晶界腐蚀。图 1为 NdFeB磁体在潮湿气氛中的腐蚀机制示意图[14]。

Li等[15]研究了 NdFeB磁体在 335～500 ℃温度范围内空气中氧化动力学行为。图 2[16]是 NdFeB磁体在 500 ℃, 24 h氧化后的背散射电子 SEM形貌图,可以看出在磁体表面有约 40 μm厚、连续分布的灰色层,如箭头标注所示,另外在灰色层外有一层厚度约为 1 μm的黑色层 (图 2(b))。图 3是 NdFeB磁体在 410 ℃, 48 h氧化后表面的 TEM照片,显示出了两层外表面氧化层和部分内部氧化区域,结合 XRD测试结果,表明外表面氧化层中的黑色层 Fe_2O_3,灰色层为 Fe_3O_4。其中导致 NdFeB磁体腐蚀失效的主要过程是磁体内部区域的氧化,且内部氧化区的深度与暴露时间成抛物线性关系,即与时间的平方根成正比。

综上所述,NdFeB磁体的腐蚀失重有两种机制:一是氧化剥落,二是吸氢粉化,究竟是哪一种占主导地位,现在还在研究之中。笔者认为,这两者都对磁体的腐蚀失重起作用,但在特定的环境条件下,可能是以某种机制的作用为主。

2　低失重烧结钕铁硼制备方法研究

NdFeB 材料的腐蚀主要表现为主相晶粒之间的晶间腐蚀，其腐蚀原动力在于主相与富钕相、富硼相之间的化学电动势差。因此，从合金的成分设计着手，要改善晶间相的成分、腐蚀电位和导电性，尽量减少不同相之间的腐蚀电位差，避免或者减弱晶间腐蚀，降低腐蚀电流密度。

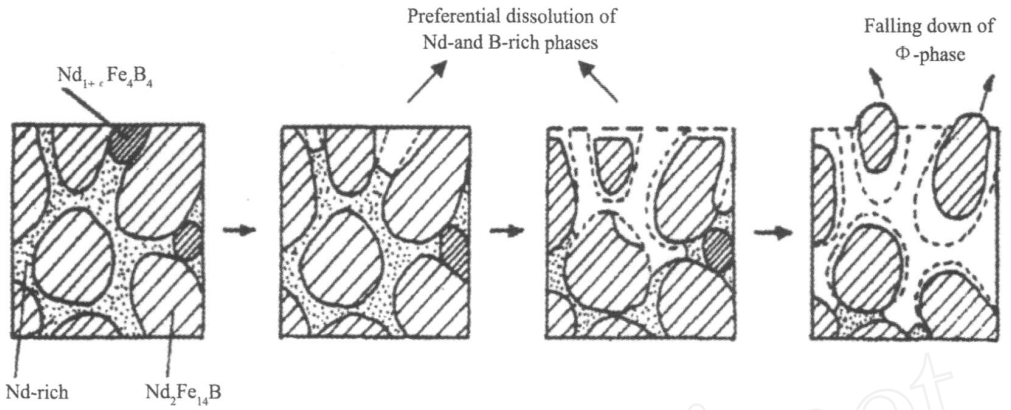

图 1　NdFeB 磁体在潮湿气氛中的腐蚀机制示意图

Fig. 1　Corrosion mechanism map of NdFeB magnets in humid environments

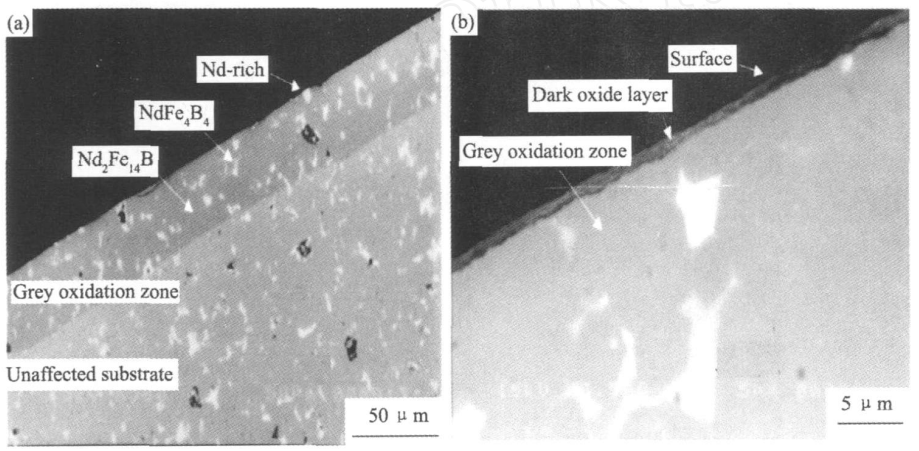

图 2　NdFeB 磁体在 500 ℃，24 h 氧化后的背散射电子 SEM 照片[16]

Fig. 2　Back scattered SEM of NdFeB magnets after oxidation at 500 ℃ for 24 h

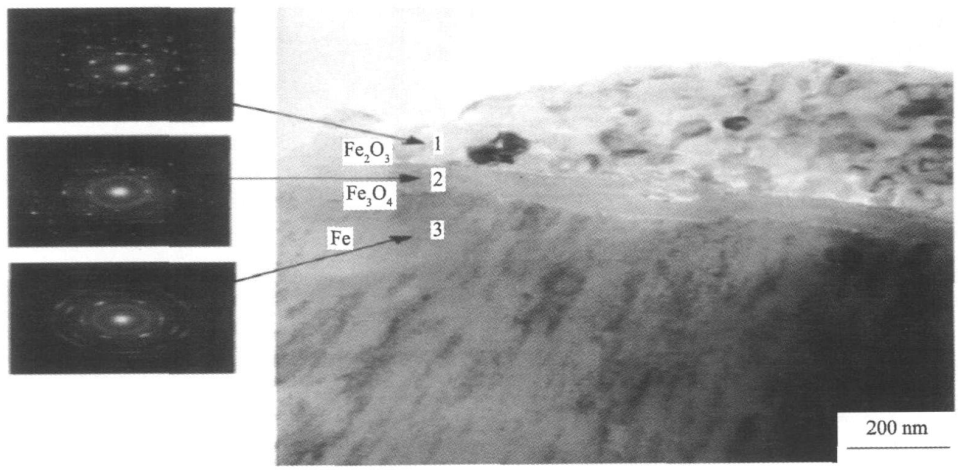

图 3　NdFeB 磁体在 410 ℃，48 h 氧化后表面层的 TEM 照片[16]

Fig. 3　The surface TEM of NdFeB magnets after oxidation at 410 ℃ for 48 h

2.1 合金化法

通过对磁体中稀土总含量与氧含量对大块烧结 Nd-Fe-B系永磁材料氧化速度的影响的研究表明，磁体的腐蚀速度随稀土总含量的降低而降低，随氧含量的升高而降低[17,18]。采用添加元素的方法影响 Nd-Fe-B系永磁材料氧化行为已经有大量的研究报道。文献[19]中提到，根据 Fidler的研究，将 NdFeB磁体的掺杂元素分为两类：M1 = (Al, Cu, Zn, Ga, Ge, Sn)低熔点合金元素；M2 = (V, Mo, W, Nb, Ti, Zr)高熔点合金元素。其中第一类形成 Nd-M_1或 Nd-M_1-Fe晶间相，第二类形成 M_2-B或 Fe-M_2-B晶间相。与没有掺杂时的相相比，这些在晶间区形成的新相具有较正的腐蚀电位，可以减弱晶间区相的反应分解，延缓晶界腐蚀的产生。Bala等[20]研究了 1%～6% Al(原子分数)的添加对 NdFeB磁体耐腐蚀性的影响，研究表明 Al的加入能够形成钝化膜，抑制磁体在空气中的进一步氧化。Femengel等[21]的研究表明通过添加元素 Co可以形成某些晶间相，尤其是 Nd_3Co相具有更高的化学稳定性，当 Co的掺入量达到3.5%时，能够改善 NdFeB磁体的耐腐蚀性能。文献[16]中提到，根据山本等的研究，在烧结钕铁硼成分内加入 Zr，V，Nb，Ta，Mo，W，Al的一至二种(不超过 2%)取代 Fe，可改善磁体的耐蚀性；Ma，Yu和 El-Moneim[22~24]亦认为在烧结磁体内加入 Nb，Ta，V，Ti，Al的 1或 2种元素，使之在晶界上偏析，减少晶界上富稀土相而提高晶界的耐氧化腐蚀性能。Teyaert等[25]研究了添加元素 (Al，Co，V，Nb，Mo)后 NdFeB磁体的氧化腐蚀行为，提到元素 V在晶界形成 $(V_{1-x}Fe_x)_3B_2$沉淀相并夹杂有 Fe-V沉淀颗粒。Mo则形成 $(Mo_{1-x}Fe_x)_3B_2$沉淀化合物，添加 Co以后，在富钕晶界相中形成含 Co的富钕相或 Nd_3Co。这些金属间化合物在晶界上部分地取代了富钕晶界相，改善了富钕晶界相的耐腐蚀性差的弱点，一定程度上提高了磁体的耐腐蚀性。同时 Al和 Co也会取代 $Nd_2Fe_{14}B$相中的 Fe的位置，它们的取代对于主相在 200 ℃以上的氧化腐蚀行为起到了较大的抑制作用。Kim的研究工作表明[26]，在烧结 Nd-Fe-B中添加 1% (原子分数) Cr后，可提高其抗腐蚀性能，这是因为 Cr进入了 $Nd_2(Fe,Cr)_{14}B$相，提高了基体的抗氧化能力。Kim的另一项研究表明[27]，在 (Nd，Dy) FeB合金中适当的添加微量的 Cu，Co和 O可以在不降低剩磁的前提下，大幅度提高磁体的矫顽力和耐腐蚀性能，如表1所示。他们还发现含有高 C，N，O的磁体具有较好的耐蚀性，他们认为当氧含量为 0.6%～1.2%，炭含量为 0.06%～0.14%，氮含量为 0.05%～0.1%磁体的失重达到最小[28]。其原因是磁体中 C，N，O元素增加后晶界相的化学稳定性增加，从而减缓了晶间腐蚀。Grieb[29]的研究表明，在 30%稀土含量的钕铁硼磁体中添加一定量的 Dy，Co，Al，Ga，Nb和 Cu可以提高耐腐蚀性和高使用温度下稳定性。显微结构观察显示，在晶界处形成了稳定的金属间化合物，它们包围着主相，并且相当光滑，同时在晶界处没有发现 Nd_3Co，NdCu和 $Nd_{1+\varepsilon}Fe_4B_4$相化合物，富钕相的含量也很少，这种大量稳定金属间化合物的存在是其失重降低的主要原因。

2.2 双合金法

用双合金法生产的钕铁硼材料的抗腐蚀性能显著的比单合金法优越。主要通过双合金法使晶界相富集 M_1等低熔点化合物相和 M_2等高熔点化合物相，这些化合物在晶界处和晶界交汇处形成稳定的金属间化合物，提高了晶界的抗腐蚀能力。双合金法能使富 Nd相在主相 $Nd_2Fe_{14}B$晶粒周围均匀包覆，并且相当光滑和平整，减少了富 Nd相的含量，也提高了磁体耐腐蚀性能。

2.3 其他因素影响烧结钕铁硼失重的研究

Bala[30]研究认为，对钕铁硼而言在硫酸介质中会产生异常溶解，即在阴极极化下具有剩磁的材料溶解速率更低。而 Costa等[31]研究表明，磁化

表 1 $Nd_{33}B_{1.1}Co_xCu_yFe_{65.9-x-y}$磁体的腐蚀失重(反应釜试验 110～115 ℃×96 h)

Table 1 Corrosion rates (weight loss) of $Nd_{33}B_{1.1}Co_xCu_yFe_{65.9-x-y}$ magnets after autoclave tests at 110～115 ℃ for 96 h

Co/%	Cu/%	Loss weight/(mg·cm^{-2})
0	0	203.3
5.0	0	17.5
0	0.15	18.3
1.2	0.15	0.15

状态下的烧结钕铁硼磁体在 NaCl介质中的腐蚀失重更大。郑精武等[32]对剩磁状态下钕铁硼在活化介质或易钝化介质中的腐蚀行为及腐蚀机制的系统性研究，认为在硫酸和氯化钠介质中，剩磁场提高了烧结钕铁硼磁体的腐蚀速率，这是因为剩磁促进具有自催化作用的闭塞腐蚀电池的形成；在磷酸和氢氧化钠介质中因形成钝化膜使得剩磁场降低，使烧结钕铁硼磁体的腐蚀速率降低。

3　结　论

综上所述，提高烧结钕铁硼磁体的自身抗腐蚀性能，降低失重，主要从磁体的成分设计和微观组织入手，其关键方面是对晶界相的成分和微观结构进行合理的控制。从理论上可以总结以下几条原则：(1) 减小晶界相腐蚀电位与主相腐蚀电位差，从而降低晶间腐蚀；(2) 增大晶界相电阻，从而减小晶界相腐蚀电流；(3) 添加的晶界相最好也是单相合金，这样在熔炼、粗破碎和制粉过程中其自身受到的大气腐蚀相对较弱；(4) 能满足磁体对晶界相的要求，熔点较低，润湿性较好，在液相烧结过程中能起到光滑主相晶粒，细化结晶，使得晶界相分布均匀，减弱磁交换耦合作用；(5) 其本身是非铁磁性的；(6) 晶界相中的某些元素在液相烧结中能通过扩散作用进入 $Nd_2Fe_{14}B$ 主相的组织中，部分取代 Nd或 Fe而改善磁体主相的耐腐蚀性能。同时利用双合金法工艺生产的磁体，晶间腐蚀较弱，同时由于辅相润湿性增加和烧结过程颗粒流动性增强，磁体的致密度增加孔隙较少，在后加工过程中受到的腐蚀也较小，最后采用表面处理得到的磁体的腐蚀失重也会更小。

参考文献：

[1] Bala H, Pawlowska G, Szymura S, Rabinovich Y M. Electrochemcail corrosion characterization of intermetallic phases occurring in Nd-Fe-B type magnets [J]. British Corrosion Journal, 1998, (1): 37.

[2] Zhang Jingxian, Zhang Tongjun, CuiKun. The mechanism of corrosion and protection of NdFeB permanent magnetic material [J]. Materials Development and Application, 2001, (4): 38.
(张静贤，张同俊，崔　琨. NdFeB永磁材料腐蚀机理与防护 [J]. 材料开发与应用，2001, (4): 38.)

[3] Verdier M, Morros J, Pere D. Stability of Nd-Fe-B powders obtained by hydrogendecrepitation [J]. IEEE Trans Magn., 1994, (2): 657.

[4] Ram S, Claude E, Joubert J C. Synthesis, stability against air and moisture corrosion, and magnetic properties of finely divided loose $Nd_2Fe_{14}BH_x$, $x < 5$, hydridepowders [J]. IEEE Trans Magn., 1995, (3): 2200.

[5] Cygan D F, Mcnallan M J. Corrosion of NdFeB permanent magnets in humidenvironments at temperatures up to 150 ℃ [J]. J. Magn. Magn. Mater., 1995, (1/2): 131.

[6] Kim A S, Camp F E, Lizzi T. Hydrogen induced corrosion mechanism in NdFeB magnets [J]. J. Appl. Phys, 1996, (8): 4840.

[7] Otaigbe J U, Xiao J, Kim H. Influence of filler surface treatments on processability andproperties of polymer-bonded Nd-Fe-B magnets [J]. J. Mater. Sci. Lett, 1999, (4): 329.

[8] Willman C J, Narasimhan K S V L. Corrosion characteristics of RE-Fe-B permanentmagnets [J]. J. Appl. Phys, 1987, (8): 3766.

[9] Chang K E, Warren G W. The electrochemical hydrogenation of NdFeB sintered alloys [J]. J. Appl. Phys, 1994, (10): 6262.

[10] Chang K E, Warren G W. The effect of absorbed hydrogen on the corrosion behavior of NdFeB alloys [J]. IEEE Trans Magn., 1995, (6): 3671.

[11] Yan G, Williams A J, Farr J P G, Harris I R. The effect of density on the corrosion of NdFeB magnets [J]. J. Alloy. Compd., 1999, (1/2): 266.

[12] Minowa T, Yoshikawa M, Honshima M. Improvement of the corrosion resistance on Nd-Fe-B magnet with nickel plating [J]. IEEE Trans Magn., 1989, (5): 3776.

[13] Zhang Shouming, Zhou Yongqia. Corrosion prevention of Nd-FeB magnet [J]. Material Protection, 1999, (9): 28.
(张守民，周永治. NdFeB磁体防腐蚀研究 [J]. 腐蚀与防护，1999, (9): 28.)

[14] Schultz L, El-Aziz A M, Barkleit G, Mummert K. Corrosion behaviour of Nd-Fe-B Permanent magnetic alloys [J]. Mater. Sci. Eng. A, 1999, (2): 307.

[15] Li Y, Evans H E, Harris I R, Jones I P. The oxidation of Nd-FeB magnets [J]. Oxid. Met., 2003, (1/2): 167.

[16] Hua Hongci. Oxidation corrosion and protection of NdFeB permanent magnetic material [A]. Electrical Engineering Materials [C]. 1991, (4): 6.
(华宏慈. 钕铁硼永磁材料的氧化腐蚀及防护 [A]. 电工合金文集 [C]. 1991, (4): 6.)

[17] Ma B M, Yl, Sott D W, Bounds C D. A new aspect on the corrosion resistance of sintered Nd-Fe-B magnets-Is high oxygen content [A]. Proc. 13th Int, Workshop on Rare Earth Magnets and Their Application [C]. 1994. 309.

[18] Kim Y B, Kim M J, Yang J H, Ryu K S, Li Ying, Kim T K.

Effects of Nd/Fe ratio on the icrostructure and magnetic properties of NdFeB thin films [J]. J. Magn. Magn. Mater., 2001, (234): 489.

[19] El-Aziz A M, Kirchner A, Gutfleisch O, Gebert A, Schultz. Investigations of the orrosion behaviour of nanocrystalline Nd-Fe-B hot pressed magnets [J]. J. Alloy. Compd., 2000, (2): 299.

[20] Bala H, Szymura S, Owczarek E, Nowy-Wiechula W. Corrosion behaviour of sintered Nd-(Fe, Al)-B magnets [J]. Intermetallics, 1997, (7): 493.

[21] Fernengel W, Rodewald W, Blank R, Schrey P, Katter M, Wall B. The influence of Co on the corrosion resistance of sintered Nd-Fe-B magnets [J]. J. Magn. Magn. Mater., 1999, (196/197): 288.

[22] Ma Y G, Li R S, Yang Z, Matsumoto M, Morisako A, Takei S. Effects of additive elements (Cu, Zr, Al) on morphological and magnetic properties of NdFeB thin films with perpendicular magnetic anisotropy [J]. Mater. Sci. Eng. B, 2005, (117): 287.

[23] Yu L Q, Wen Y H, Yan M. Effects of Dy and Nb on the magnetic properties and corrosion resistance of sintered NdFeB [J]. J. Magn. Magn. Mater., 2004, (283): 353.

[24] El-Moneim A A, Gebert A, Uhlemann M, Gutfleisch O, Schultz L. The influence of Co and Ga additions on the corrosion behavior of nanocrystalline NdFeB magnets [J]. Corros. Sci., 2002, (44): 1857.

[25] Teyaert S, Le Breton J M, Teillet J. Microstructure and corrosion resistance of Nd-Fe-B magnets containing additives [J]. J. Phys. D. Appl. Phys., 1998, (31): 1534.

[26] Kim A S. High performance, temperature stable and corrosion resistant Nd-Fe-B magnets [A]. Proc. 3rd. Int. Symp. on Physics of Magnetic Materials (ISPMM'95) [C]. Seoul, Korea, 1995. 646.

[27] Kim A S, Camp F E. High performance NdFeB magnets (invited) [J]. J. Appl. Phys., 1996, (8): 5035.

[28] Kim A S, Camp F E, Dulis E J. Effect of oxygen, carbon, nitrogen contents on the corrosion resistance of Nd-Fe-B magnets [J]. IEEE Trans. Magn., 1990, 26: 1936.

[29] Grieb B. New corrosion resistant materials based on neodym-iron-boron [J]. IEEE Trans. Magn., 1997, (5): 3904.

[30] Bala H, Szymura S. Corrosion Science, 1991, 32(9): 953.

[31] Costa I, Oliveira M C L, deMelo H G. Journal of Magnetism and Magnetic Materials, 2004, 278: 348.

[32] Zheng Jingwu, Du Zhouyun, Jiang Meiyan, Qiao Liang, Jiang Liqiang, Zhang Cheng. Corrosion behavior of Nd-Fe-B sintered magnets at remanence state [J]. Rare Metal Materials and Engineering, 2008, 37(8): 1369.

(郑精武, 都周云, 蒋梅燕, 乔 梁, 姜力强, 张 诚. 烧结钕铁硼在剩磁状态下的腐蚀研究 [J]. 稀有金属材料与工程, 2008, 37(8): 1369.)